

What drives the HI content of central galaxies - A comparison between hydrodynamic simulations and observations using Random Forest

XIAO LI,¹ CHENG LI,¹ AND H. J. MO²

¹*Department of Astronomy, Tsinghua University, Beijing 100084, China*

²*Department of Astronomy, University of Massachusetts Amherst, MA 01003, USA*

ABSTRACT

We investigate the driving mechanisms for the HI gas content in star-forming central galaxies at low redshift, by examining the HI-to-stellar mass ratio (M_{HI}/M_*) in both the state-of-the-art hydrodynamic simulations, IllustrisTNG (TNG) and EAGLE, and the xGASS sample. We quantify the correlations of M_{HI}/M_* with a variety of galaxy properties using the random forest regression technique, and we make comparisons between the two simulations, as well as between the simulations and xGASS. Gas-phase metallicity is found to be most important in both simulations, but is ranked mildly for xGASS, suggesting that metals and gas driven by feedback effects in real galaxies is not as tightly coupled as in the simulations. Beyond that, the accretion rate of supermassive black holes is the most important feature in TNG, while specific star formation rate is the top ranked in EAGLE. This result can be understood from the fact that the HI gas is regulated mainly by thermal-mode AGN feedback in TNG and by stellar feedback in EAGLE. Although neither simulation can fully reproduce the feature importance obtained for real galaxies in the xGASS, EAGLE performs better than TNG in the sense that the observationally top-ranked property, $u-r$, is also highly ranked in EAGLE. This result implies that stellar feedback plays a more dominant role than AGN feedback in driving the HI gas content of low-redshift galaxies.

Keywords: dark matter halo – atomic hydrogen – interstellar medium

1. INTRODUCTION

In current models, galaxies form at the center of dark matter halos through cooling and condensation of gas (White & Rees 1978; Mo et al. 2010). Theoretically, gas-related processes in/around galaxies have been extensively studied in the past decade with the help of cosmological hydrodynamic simulations, such as Horizon-AGN (Dubois et al. 2012), Magneticum¹, EAGLE (Crain et al. 2015; Schaye et al. 2015), FIRE (Hopkins 2015; Hopkins et al. 2014), Illustris (Vogelsberger et al. 2014a,b; Sijacki et al. 2015; Genel et al. 2014), IllustrisTNG (Springel et al. 2018; Naiman et al. 2018; Marinacci et al. 2018; Nelson et al. 2018; Pillepich et al. 2018), and SIMBA

(Davé et al. 2019). In particular, many efforts have been made to investigate atomic hydrogen (HI), the dominant component of cold gas. These simulations are usually able to reproduce the abundance of galaxies as a function of the HI mass and the HI size-mass relation in the local Universe (e.g. Bahé et al. 2016; Crain et al. 2017; Diemer et al. 2019; Ma et al. 2022). However, the simulations have also shown that the HI content of a galaxy can be regulated by a variety of processes, including consumption by star formation (Springel & Hernquist 2003; Schaye & Dalla Vecchia 2008; Hopkins et al. 2014), heating or outflows by stellar feedback (Pillepich et al. 2018; Dalla Vecchia & Schaye 2012; Hopkins et al. 2014) and active galactic nucleus (AGN) feedback (Booth & Schaye 2009; Dubois et al. 2012; Weinberger et al. 2017), and tidal or ram-pressure stripping by surrounding hot gas and companion galaxies (Marasco et al. 2016; Stevens et al. 2019; Watts et al. 2020). Different simulations use different mechanisms to reproduce the observations of HI gas, and it is unclear which mechanisms drive the HI mass and distribution in real galaxies. For instance,

Corresponding author: Xiao Li
xli27938@gmail.com

Corresponding author: Cheng Li
cli2015@tsinghua.edu.cn

¹ <http://www.magneticum.org/simulations.html>

using *EMP-pathfinder* (Reina-Campos et al. 2022) and FIREbox (Feldmann et al. 2023), Gensior et al. (2024) showed that different subgrid physics can result in consistent galaxy-wide HI properties, but the small-scale properties are very different, with the rotational asymmetry of the HI discs has the strongest dependence on the physical processes implemented.

On the observational side, large HI surveys accomplished in the past two decades, such as HI Parkes All-Sky Survey (HIPASS; Meyer et al. 2004) and Arecibo Legacy Fast ALFA survey (ALFALFA; Giovanelli et al. 2005), have greatly advanced our understanding of HI gas properties in local galaxies. These include the abundance of HI-rich galaxies as quantified by the HI mass function (HIMF; Zwaan et al. 2005; Martin et al. 2010; Jones et al. 2018), the dependence of galaxy clustering on HI mass (Meyer et al. 2007; Martin et al. 2012; Papastergis et al. 2013; Guo et al. 2017), the scaling relations of HI mass fraction with various galaxy properties (Kannappan 2004; Zhang et al. 2009; Li et al. 2012; Huang et al. 2012; Catinella et al. 2010; Obreschkow et al. 2016; Catinella et al. 2018; Zu 2020; Li et al. 2022; Lu et al. 2024), and the HI-to-halo mass relation for both central galaxies and all the galaxies in dark matter halos (Hess & Wilcots 2013; Barnes & Haehnelt 2014; Guo et al. 2017; Paul et al. 2018; Villaescusa-Navarro et al. 2018; Obuljen et al. 2019; Guo et al. 2020; Chauhan et al. 2020; Calette et al. 2021; Chauhan et al. 2021; Li et al. 2022; Rhee et al. 2023; Saraf et al. 2024). Furthermore, the HI scaling relations provide an economic but reliable way to estimate the HI mass fraction for optically-selected galaxy samples that are much deeper and larger than the existing HI surveys. This allows the abundance and clustering of HI-selected galaxies to be measured more accurately and over larger dynamical ranges of galaxy properties. For instance, by applying an improved estimator to the galaxy sample from the Sloan Digital Sky Survey (SDSS; York et al. 2000), Li et al. (2022) obtained the first estimates of the conditional HI mass functions (CHIMFs), that is, HIMFs for galaxies hosted by dark matter halos of given mass.

The observations of HI should in principle provide useful constraints on the subgrid physics implemented in hydrodynamic simulations. For instance, Davé et al. (2020) found that SIMBA well reproduces the HIMF at $z = 0$, but overestimates the HI fraction of massive galaxies, implying too strong a jet-mode AGN feedback which plays a major role in regulating the HI gas content in this simulation. For IllustrisTNG, the HI mass of central galaxies is found to have no or weak correlation with star formation rate (SFR; Ma et al. 2022), in contrast to the tight correlation between HI mass frac-

tion and SFR in real galaxies. In Li et al. (2022), the comparison of the HI-to-halo mass relation between observations and simulations show that both Illustris and IllustrisTNG simulations significantly overpredict the HI mass for both the central galaxy and all the galaxies as a whole at fixed halo mass. Due to the complex subgrid physics in the simulations, as mentioned above, it is not immediately clear what causes the agreement and disagreement between simulations and observations.

In this work, we adopt the random forest algorithm (Breiman 2001) to investigate the driving processes for the HI gas content in IllustrisTNG (hereafter TNG) and EAGLE. Both TNG and EAGLE are state-of-the-art hydrodynamic simulations, but they implement very different feedback models, thus allowing a comparison of the effects of different feedback processes on the HI contents of galaxies. Random forest is a widely-used machine learning algorithm that is able to efficiently identify the most important feature with respect to the target from a large parameter space (e.g. Bluck et al. 2022, 2023; Baker et al. 2023; Ellison et al. 2024; Goubert et al. 2024; Jing & Li 2024; Li & Li 2024). We consider galaxy properties that are previously found to be correlated with HI mass fraction (e.g., specific SFR, color, stellar mass, stellar surface density, gas metallicity), as well as other properties that are potential tracers of important gas-related processes (e.g., black hole mass and accretion rate). We then compare the importance pattern of the properties in simulated galaxies with that identified in the same way from the observed galaxies in the xGASS survey, aiming to find out the driving mechanisms for the HI mass fraction in low-redshift galaxies.

This paper is organized as follows. In section 2 we first perform the random forest analysis for the two simulations. In section 3 we then perform the same analysis for the xGASS galaxy sample and make comparisons between the simulations and the observational results. Finally, we summarize our work in section 4.

2. RANDOM FOREST ANALYSIS OF SIMULATIONS

2.1. Data and Sample Selection

2.1.1. IllustrisTNG

The IllustrisTNG project (Springel et al. 2018; Naiman et al. 2018; Marinacci et al. 2018; Nelson et al. 2018; Pillepich et al. 2018, hereafter TNG) is a suite of cosmological magneto-hydrodynamic simulations in a Λ CDM universe run with the moving-mesh code AREPO (Springel 2010). To ensure both resolution and volume, in this work we use the publicly available TNG100 data, which has a box length of $75 h^{-1}$ Mpc and a baryonic mass resolution of $1.4 \times 10^6 M_{\odot}$. IllustrisTNG adopts

the cosmological parameters from [Planck Collaboration et al. \(2016\)](#): $\Omega_m = 0.3089$, $\Omega_b = 0.0486$, $h = 0.6774$, and $\sigma_8 = 0.8159$. The galaxy formation and evolution models in IllustrisTNG simulations include gas cooling, star formation, galactic winds, metal enrichment, supernovae, black hole growth, active galactic nuclei (AGN) feedback ([Weinberger et al. 2017](#); [Pillepich et al. 2018](#)), and magnetic field. Dark matter halos are identified using FoF algorithm ([Davis et al. 1985](#)). Then the SUBFIND algorithm ([Springel et al. 2001](#)) is used to identify subhalos (galaxies) in FoF halos.

2.1.2. EAGLE

The EAGLE project ([Crain et al. 2015](#); [Schaye et al. 2015](#)) is a suite of hydrodynamic simulations in a Λ CDM universe. EAGLE was run using a modified version of the N -Body Tree-PM smoothed particle hydrodynamics (SPH) code GADGET3, originally developed by [Springel \(2005\)](#). The simulations adopt the cosmological parameters from [Planck Collaboration et al. \(2014\)](#): $\Omega_m = 0.307$, $\Omega_b = 0.0483$, $h = 0.6777$, and $\sigma_8 = 0.8288$. In this work we use the fiducial simulation Ref-L100N1504, which has a volume of side $L = 100$ Mpc and a baryonic particle mass of $1.81 \times 10^6 M_\odot$. The subgrid processes implemented in Ref-L100N1504 include radiative cooling, reionization, star formation, chemical enrichment, supernova feedback, black hole growth, and AGN feedback. Dark matter halos and subhalos are identified using the FoF and SUBFIND algorithms, respectively.

2.1.3. HI/H₂ Partition Models

Both TNG and EAGLE output only the total mass of hydrogen element in each gas particle, without providing fractions of the ionized (HII), atomic (HI) and molecular (H₂) phases. The partition between HI and H₂ is done with a post-processing procedure, which is similar in the two simulations. The hydrogen gas is first divided into ionized and neutral phases, and models of the HI/H₂ partition are then applied to the neutral phase to estimate the mass fraction of HI and H₂ gas. Both simulations implemented multiple models for the HI/H₂ partition. As described in [Bahé et al. \(2016\)](#), EAGLE applied the HI/H₂ models of [Blitz & Rosolowsky \(2006\)](#) (BR06) and [Gnedin & Kravtsov \(2011\)](#) (GK11). For TNG, as described in [Diemer et al. \(2018\)](#), the HI/H₂ partition is obtained by using the models of [Leroy et al. \(2008\)](#) (L08), [Gnedin & Kravtsov \(2011\)](#) (GK11), [Krumholz \(2013\)](#) (K13), [Gnedin & Draine \(2014\)](#) (GD14), and [Sternberg et al. \(2014\)](#) (S14). In most models the HI/H₂ partition is based on gas surface density, which is not naturally available in hydrodynamic simulations. In

TNG, the gas surface density is estimated in two different ways, either by multiplying the volume density with the Jeans length (the volumetric (vol) method), or by projecting the gas cells along the direction of the gas angular momentum (the projected (map) method). In EAGLE, the HI and H₂ gases are assumed to have the same scale height so that the ratio of surface densities of H₂ and HI is the same as the ratio of their volume densities.

2.1.4. Galaxy Properties

We consider the following galaxy properties for the random forest analysis of the simulations:

- $\log M_*$: the logarithm of the stellar mass, in units of solar mass. This is the sum of masses of all stellar particles within 30 kpc. A fixed aperture of 30 kpc is demonstrated to track the Petrosian radii used in observations ([Schaye et al. 2015](#)).
- $\log \mu_*$: the logarithm of the stellar surface mass density, defined by $\mu_* \equiv M_*/(2\pi R_e^2)$, where R_e is the half stellar mass radius in units of kpc.
- $\log \text{sSFR}$: the logarithm of the specific star formation rate, defined as $\log \text{SFR}/M_*$, where SFR is the instantaneous star formation rate calculated using all the star-forming gas elements belonging to the subhalo for EAGLE galaxies and using star-forming gas cells within 2 times of the half stellar mass radius for TNG galaxies.
- $\log \sigma_*$: the logarithm of the stellar velocity dispersion. For EAGLE galaxies, σ_* is the one-dimensional velocity dispersion of all stellar particles. For TNG galaxies, σ_* is approximated using the one-dimensional velocity dispersion of all subhalo member particles.
- $u - r$: color index defined by the difference in absolute magnitude between u and r band. The absolute magnitudes are calculated using stellar population synthesis models with dust obscuration taken into account ([Trayford et al. 2015](#); [Nelson et al. 2018](#)).
- $\log(\text{O}/\text{H}) + 12$: gas phase metallicity of star forming gas. This is calculated using all the star-forming gas elements belonging to the subhalo for EAGLE galaxies and star-forming gas cells within 2 times of the half stellar mass radius for TNG galaxies.
- $\log M_{\text{BH}}$: the logarithm of the mass of the central supermassive black hole, in units of M_\odot .

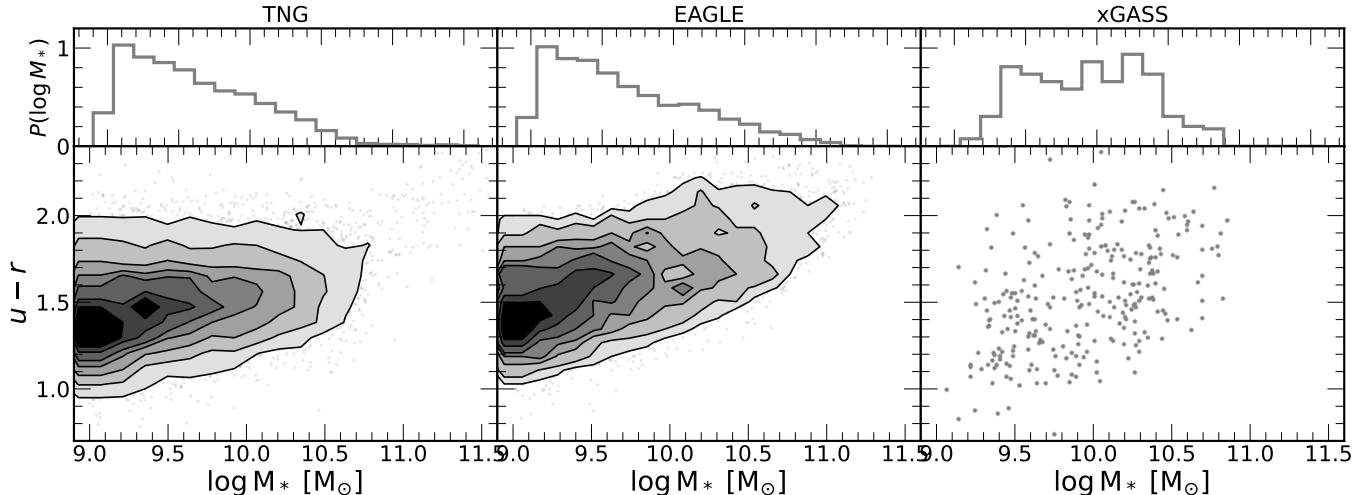


Figure 1. Bottom panel: The color-mass diagram of TNG, EAGLE, and xGASS sample used in this work. The grey contours show the distribution of simulation samples. Contours from inner-most to outer-most include 10%, 25%, 40%, 55%, 70%, 85%, and 95% of the total sample. Galaxies outside the outer-most contour are denoted as small grey dots. **Upper panel:** The normalized stellar mass distribution of TNG, EAGLE, and xGASS sample.

- $\log \dot{M}_{\text{BH}}$: the logarithm of the accretion rate of the central supermassive black hole, in units of M_{\odot}/yr .
- $\log V_{\text{max}}$: the logarithm of the maximum value of the spherically-averaged rotation velocity, in units of km/s.
- $\log Z_{*}$: the logarithm of the stellar metallicity, derived from all stellar member particles in EAGLE, and from stellar member particles within twice the half stellar mass radius in TNG.

We note that, in both EAGLE and TNG, the HI mass is measured using an aperture of 70 kpc, and the stellar mass is measured within 30 kpc for the consistency of sample selection. For all other properties, we directly take the measurements from the subhalo catalogs, publicly available through the websites of the two simulations². For the star formation rate and gas metallicity, EAGLE considers all gas particles belonging to the subhalo, while TNG only considers gas cells belonging to the subhalo within twice the half stellar mass radius (R_e). Star-forming gas is expected to concentrate in the inner region, mostly within $2R_e$. In addition, the feature importance analysis is sensitive to the ranking but not the absolute value of the properties considered. For these reasons, the small differences in property definitions are expected to have negligible effects on the results presented in this work.

² EAGLE: <https://icc.dur.ac.uk/Eagle/database.php>; TNG: <https://www.tng-project.org/data/>

2.1.5. Sample Selection

Our investigation focuses on star-forming central galaxies, for the following two considerations. First, most of the quenched galaxies do not have reliable HI gas measurements due to the limited mass resolution of the simulations. Second, the HI content of satellite galaxies is known to suffer from environmental effects such as ram-pressure stripping and tidal stripping, making it hard to reliably assess the importance of properties internal to the galaxies. We will come back and study the effect of environments in the future. Here, we select star-forming central galaxies with stellar mass $M_{*} > 10^9 M_{\odot}$ and specific star formation rate $\log \text{sSFR} > -11$. To avoid unreliable HI gas measurements, we further require the HI-to-stellar mass ratio to be larger than a fixed limit: $\log M_{\text{HI}}/M_{*} > -2$. These restrictions give rise to a sample of 10,205 galaxies from TNG, and a sample of 6,287 galaxies from EAGLE. The left two panels of Figure 1 show the distribution of sample galaxies in the $u-r$ versus $\log M_{*}$ diagram. As expected, galaxies in both samples are predominantly blue, with $u-r < 2.2$. Both samples are dominated by galaxies of low to intermediate masses, with very few galaxies with mass exceeding $10^{11} M_{\odot}$. EAGLE galaxies show a positive correlation between the color and the mass, which is not obviously seen in TNG.

2.2. Feature Importance Ranking in the Simulations

Following common practice, we use the Gini importance value provided by the random forest regressor to assess the significance of individual galaxy properties to the HI-to-stellar mass ratio. The properties used are

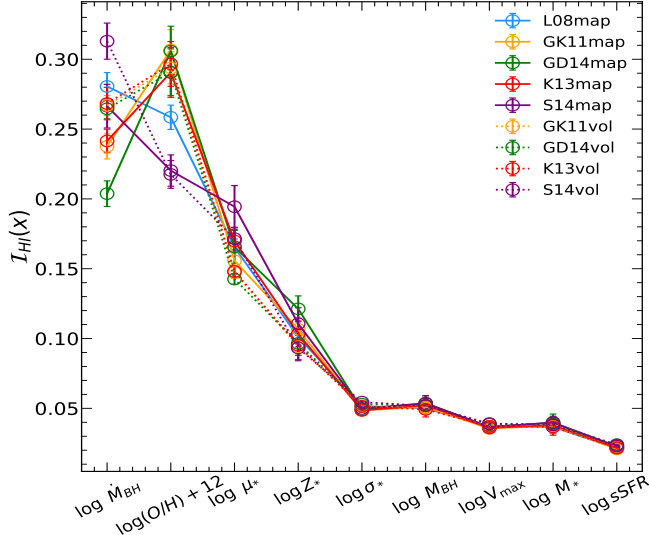


Figure 2. Feature importance of the TNG sample. The solid/dashed lines represent projected(map)/volumetric(vol) method to estimate the gas surface density. HI/H₂ partition models are denoted by different colors (blue: Leroy et al. (2008), orange: Gnedin & Kravtsov (2011), green: Gnedin & Draine (2014), red: Krumholz (2013), purple: Sternberg et al. (2014)).

listed and described in subsection 2.1.4. We use the SCIKIT-LEARN³ (Pedregosa et al. 2011) machine learning python package to realize the random forest algorithm. The importance of properties for the TNG sample is shown in Figure 2 in a decreasing order. Plotted in different colors are results for different HI/H₂ partition models, while the solid and dashed lines of the same color represent results for a given HI/H₂ partition model using two different methods to determine the gas surface density (see subsection 2.1.4). The uncertainties of the feature importance are estimated by the scatter between 40 subsamples, each constructed by randomly selecting two thirds of the galaxies from the full sample.

In all the models, the black hole accretion rate ($\log \dot{M}_{\text{BH}}$) and the gas-phase metallicity ($\log(\text{O}/\text{H}) + 12$) are ranked as the top two properties in terms of feature importance, with $\log \dot{M}_{\text{BH}}$ the most important for L08map, S14vol and S14map, and $\log(\text{O}/\text{H}) + 12$ the most important for all other models. The two properties are followed by the stellar surface mass density (μ_*) and the stellar metallicity (Z_*). The specific star formation rate, $\log \text{sSFR}$, is surprisingly ranked as the least important property, a result that is opposite to the well-known correlation between cold gas content and star for-

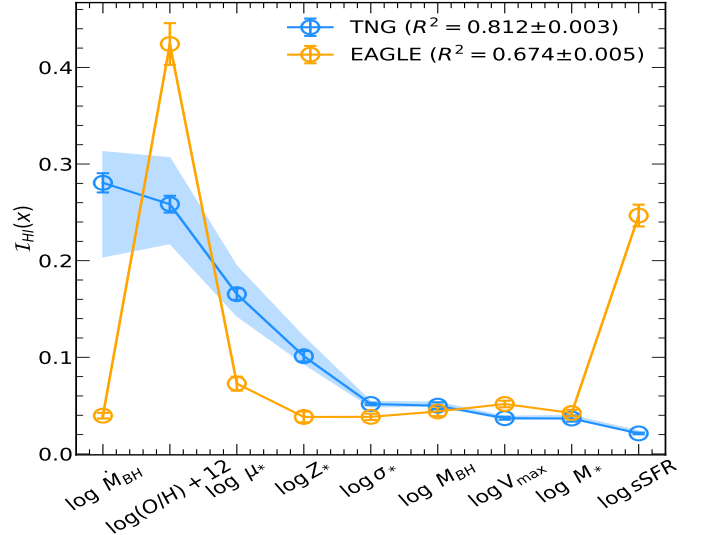


Figure 3. Feature importance of the EAGLE(orange) and TNG(blue) sample. The shaded region represents the uncertainty of feature importance due to HI/H₂ partition models. The R^2 score of each sample is shown in the legend.

mation in galaxies. Nevertheless, the results shown in Figure 2 demonstrate that the ranking of feature importance obtained from TNG is robust to the choice of HI/H₂ partition models for all the properties except between $\log \dot{M}_{\text{BH}}$ and $\log(\text{O}/\text{H}) + 12$.

For EAGLE, although two HI/H₂ partition models (BR06 and GK11) were used, the resulting HI data is publicly available only for BR06. In Figure 3, the feature importance obtained from the BR06 model are plotted as the orange circles with error bars. For comparison, the results of the different HI/H₂ partition models from TNG are plotted as the blue shaded region, with the upper and lower envelopes corresponding, respectively, to the maximum and minimum importance among all the HI/H₂ partition models for any given property. The blue circles with error bars represent the L08map model in TNG, which estimates the ratio between H₂ and HI gas surface density as a power law of midplane pressure, in the same way as the BR06 model. In what follows we will only consider the L08map model for TNG and the BR06 model for EAGLE, for simplicity.

As can be seen from Figure 3, the most important property in EAGLE is $\log(\text{O}/\text{H}) + 12$, followed by $\log \text{sSFR}$ and μ_* . This is in contrast to TNG, where $\log \dot{M}_{\text{BH}}$ is ranked the top and $\log \text{sSFR}$ the bottom. The importance of $\log \dot{M}_{\text{BH}}$ in EAGLE is nearly zero. The only similarity between the two simulations is that $\log(\text{O}/\text{H}) + 12$ is important in both. The overall difference between the two simulations is quite striking: while the HI content in EAGLE is dominated by two properties, in TNG more factors seem to be involved. This

³ <https://scikit-learn.org/stable/index.html>

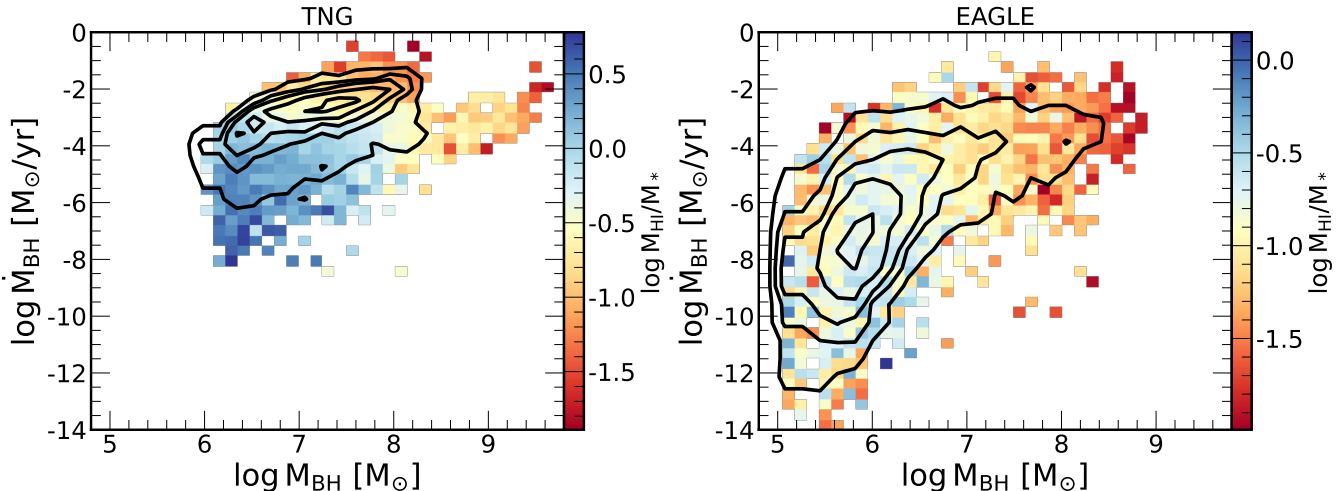


Figure 4. Black hole accretion rate as a function of black hole mass for the TNG(left) and EAGLE(right) sample, color-coded by HI fraction. The black contours show the number density distribution of the sample.

indicates that EAGLE and TNG are intrinsically different. In the following subsection, we examine sources leading to the difference between the two simulations as revealed by the feature importance of HI contents of galaxies, and show that the difference can be understood in terms of the different treatments of key subgrid processes that regulate star formation and feedback.

2.3. Implications of the Feature Importance

We first examine the correlation of the HI gas content with the black hole accretion rate. This rate is one of the most important properties in TNG but shows no importance in EAGLE. In Figure 4, we show the distribution of galaxies in the \dot{M}_{BH} versus black hole mass (M_{BH}) plane, color-coded by the HI-to-stellar mass ratio (hereafter HI mass fraction or HI/M_*). As one can see, EAGLE shows an overabundance of low mass black holes ($M_{\text{BH}} < 10^6 M_\odot$) in comparison to TNG, possibly caused by the different black hole seed mass adopted in TNG ($8 \times 10^5 h^{-1} M_\odot$) and EAGLE ($10^5 h^{-1} M_\odot$). Both simulations show a positive correlation between $\log \dot{M}_{\text{BH}}$ and $\log M_{\text{BH}}$. In TNG and below $M_{\text{BH}} \sim 10^{8.2} M_\odot$, the HI mass fraction is negatively correlated with $\log \dot{M}_{\text{BH}}$ and nearly independent of black hole mass. Above $M_{\text{BH}} \sim 10^{8.2} M_\odot$, the HI mass fraction plummets due to the onset of the kinetic mode of AGN feedback. Such a feedback prevents the cooling of gas in the CGM and the replenishment of the cold gas in ISM, leading to the quenching of star formation (Zinger et al. 2020; Piotrowska et al. 2022). In contrast, EAGLE shows only a weak negative correlation between $\log M_{\text{BH}}$ and HI mass fraction, and the value of $\log \dot{M}_{\text{BH}}$ is on average much lower than that in TNG. These results are consistent with the feature importance as found above.

In EAGLE, most of the sample galaxies have $M_* < 10^{10.5} M_\odot$, corresponding to a halo mass of $M_h \lesssim 10^{12} M_\odot$ based on the stellar-to-halo mass relation of central galaxies at $z=0$ (Wechsler & Tinker 2018). In these low-mass halos, the gas outflow driven by stellar feedback is able to escape from the host halo and to affect the CGM (Mitchell et al. 2020; Wright et al. 2024). The rate of gas inflow into the ISM is thus very low, leading to the low rate of black-hole accretion observed in Figure 4 and inefficient AGN feedback. In addition, since the AGN feedback energy in EAGLE is not released until it is high enough to increase the temperature of a neighboring gas particle by $\Delta T_{\text{AGN}} = 10^{8.5} \text{K}$ (Schaye et al. 2015; Crain et al. 2015), the feedback energy released at one time does not necessarily correspond to the accretion rate of the supermassive black hole at the same time, which may reduce the correlation between the cold gas content and the accretion rate of the central black hole. Even for galaxies with high black hole accretion rates, EAGLE does not show a significant correlation between the black hole accretion rate and the HI mass fraction, indicating that it is the pulse-like characteristic, not the low accretion rate, that is responsible for the low importance of the black hole accretion rate in EAGLE. This is consistent with the result of Ward et al. (2022) who found a weak trend of the molecular gas fraction with the luminosity of the central AGN in EAGLE and interpreted it as a consequence of the “pulsed” AGN feedback.

In contrast, most galaxies in the TNG sample are in the thermal mode of AGN feedback which continuously inject energy into the surrounding ISM, producing a strong negative relationship between the HI mass fraction and the black hole accretion rate. In addition, as

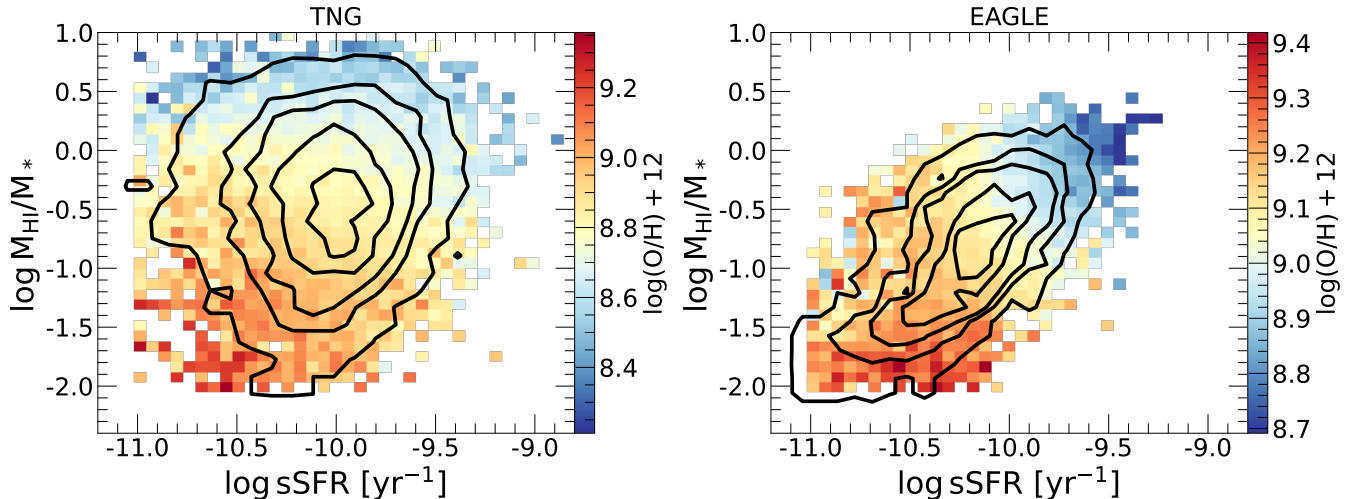


Figure 5. HI fraction as a function of specific star formation rate for the TNG(left) and EAGLE(right) sample, color-coded by gas phase metallicity of star-forming gas. The black contours show the number density distribution of the sample.

shown in [Davé et al. \(2020\)](#), the amplitude of the HIMF decreases in TNG but increases in SIMBA and EAGLE as one goes from $z = 0$ to $z = 2$. Since both TNG and SIMBA implement stellar feedback using decoupled kinetic winds, the striking difference in the evolution of the HIMF is likely caused by the thermal AGN feedback implemented in TNG, which is expected to be stronger at $z = 2$ than at $z = 0$ ([Weinberger et al. 2017](#)). [Ma et al. \(2022\)](#) and [Ward et al. \(2022\)](#) also found a notable negative correlation between the cold gas fraction and the accretion rate of the thermal mode AGN. These previous studies and our results all show that the thermal AGN feedback in TNG affects significantly the cold gas content in star-forming galaxies at $z = 0$.

Next, we examine the correlation of HI gas content with the gas-phase metallicity and sSFR. As seen from [Figure 3](#), $\log(\text{O}/\text{H}) + 12$ is identified as a very important feature in both EAGLE and TNG, while $\log \text{sSFR}$ is only important in EAGLE. [Figure 5](#) plots the HI mass fraction as a function of $\log \text{sSFR}$, with the black contours showing the number density of galaxies and the color-coding showing $\log(\text{O}/\text{H}) + 12$. As can be seen from the right panel, EAGLE galaxies show strong correlations between each pair of HI mass fraction, sSFR and gas-phase metallicity, a result that is in broad agreement with previous results ([Ellison et al. 2008](#); [Mannucci et al. 2010](#); [Bothwell et al. 2013](#); [Hughes et al. 2013](#); [Zahid et al. 2014](#); [De Rossi et al. 2017](#)). As pointed out in [Lagos et al. \(2016\)](#), these correlations are a consequence of the self-regulation of star formation, which dominates the gas-star-gas cycling for low-mass galaxies like the EAGLE galaxies studied here. In this case, the inflow of pristine gas reduces gas metallicity and triggers star formation, which in turn release feedback energy and en-

riched metals to the surrounding gas, generating gas outflows and suppressing gas inflows. Galaxies thus evolve in a quasi-static way so that gas inflow, gas outflow and star formation occur at balanced rates, producing a tight relation between star formation and cold gas mass. For massive galaxies the self-regulation of star formation is broken due to AGN feedback, driving significant deviation from the relations between gas mass, stellar mass and gas metallicity ([Zerbo et al. 2024](#)). However, many of these massive galaxies are quenched galaxies that are not selected into our sample of star-forming galaxies.

Unlike EAGLE and contrary to observations, the HI mass fraction of TNG galaxies is correlated only with gas metallicity, and shows no or weak correlation with sSFR. We find that the different behaviors of the two simulations are caused by the different fractions of HI gas that is distributed outside the galaxies. This can be seen from [Figure 6](#). The left-hand panel shows the HI mass enclosed within R_e , $2R_e$ and the radius of the host subhalo as a function of stellar mass, for both simulations. Within R_e and $2R_e$, the two simulations show similar HI-to-stellar mass relations. When the total HI gas is included, TNG galaxies have significantly larger amounts of gas outside the stellar radii, indicating more extended HI discs relative to the stellar disk. The right-hand panel further shows the ratio of the total HI mass within the host subhalo to the HI mass within $2R_e$, which quantifies how centrally concentrated the HI gas is. The ratio is roughly constant at ~ 4.5 in TNG, indicating that only one fifth of the HI gas is locked within galaxies. In contrast, the HI gas in EAGLE is more confined within galaxies, with much smaller values of the ratio at all masses. In particular, at lowest masses ($M_* \sim 10^9 M_\odot$) nearly all the HI gas in EAGLE

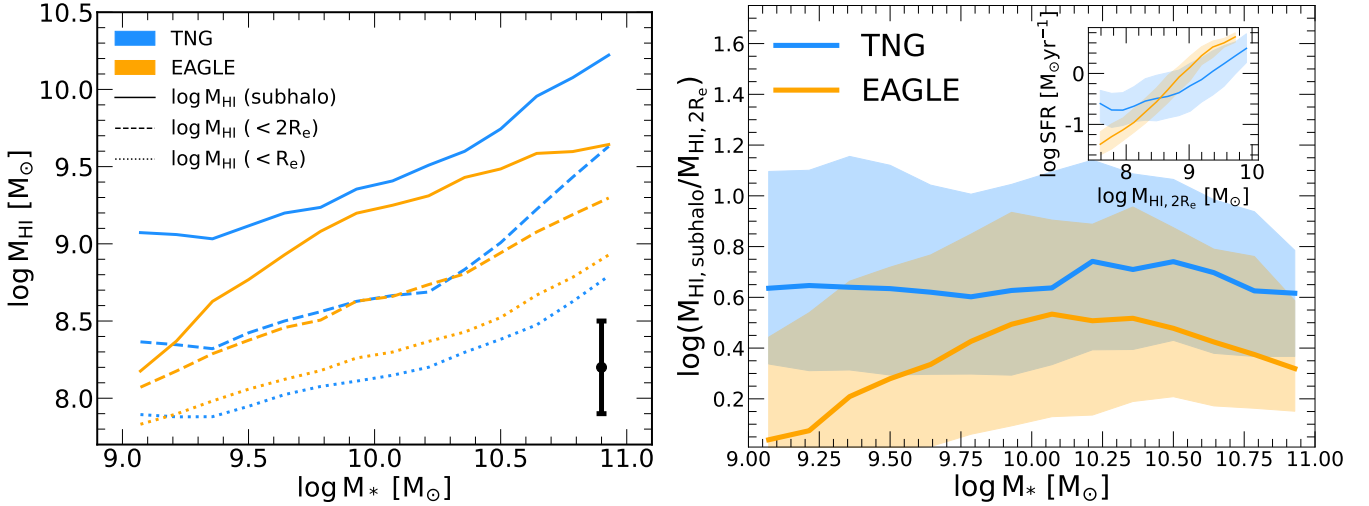


Figure 6. **Left:** The HI mass enclosed within R_e (dotted), $2R_e$ (dashed), and the radius of the host subhalo (solid) as a function of stellar mass in TNG (blue) and EAGLE (orange). The black error bar represents the typical error for clarity. **Right:** The ratio of the total HI mass within the host subhalo to the HI mass within $2R_e$ as a function of stellar mass. The shaded region represents the 1σ scatter. The inset panel shows the star formation rate as a function of the HI mass enclosed within $2R_e$.

galaxies is located within $2R_e$. Considering the SFR is calculated within $2R_e$, this result indicates that only a small fraction of HI gas contributes to star formation in TNG, thus resulting in a weak correlation between HI gas fraction and sSFR. If one only considers the HI gas within $2R_e$, as shown in the inset, the HI mass is indeed positively correlated with SFR in both simulations, although the relation in TNG shows a flatter slope and a larger scatter compared to that in EAGLE.

In summary, the above results combine to show that the HI contents in EAGLE and TNG are regulated by distinct feedback processes. In EAGLE and for galaxies of $M_* < 10^{10.5} M_\odot$, stellar feedback efficiently expels ISM gas out of host halos, leading to suppressed rates of gas inflow onto both ISM and central supermassive black hole (Mitchell et al. 2020; Davies et al. 2020) and thus a negligible effect of AGN feedback. In this case, star formation is self-regulated, leading to balance between gas outflow/inflow and star formation, and a tight correlations between SFR and HI mass fraction and stellar mass. AGN feedback is important in EAGLE only for massive halos ($M_h > 10^{12} M_\odot$) where the gravitational potential is deep enough to prevent the star formation-driven outflow (Bower et al. 2017), and so the established relation between the HI mass and the star formation rate is not destroyed by the AGN feedback in low-mass galaxies that dominate our sample.

In TNG, galactic wind driven by star formation is gentle and mostly stays within the host halo. The gas returns to the ISM and CGM after cooling (Davies et al. 2020; Ayromlou et al. 2023), forming a large and spatially extended HI reservoir (Grand et al. 2019; Diemer

et al. 2019; Yang et al. 2024). The HI-to-stellar mass ratio is weakly correlated with sSFR which is determined by the gas within $2R_e$ of the galaxy. The central supermassive black hole is able to maintain a high accretion rate, continuously heating surrounding gas via thermal AGN feedback and resulting in a strong correlation between the HI fraction and the black hole accretion rate discussed above. In more massive halos ($M_h > 10^{12} M_\odot$), AGN feedback is dominated by the kinetic mode, which can significantly reduce the CGM gas reservoir. In this case, the amounts of star formation and cold gas are both suppressed, leading to the formation of quenched galaxies that are not included in the samples of star-forming galaxies concerned here.

Despite of the very different feedback models implemented in the two simulations and their different predictions for the relation between cold gas mass and star formation rate, both simulations predict a strong correlation between the gas-phase metallicity and the HI mass fraction. Such a tight relation is expected if metals produced by star formation is well mixed in the ISM. In this case, the fractional metal loss is proportional to the fractional total-mass loss from the ISM and the ISM metallicity is determined by the remaining gas fraction even when outflows and the inflow of low-metallicity gas are involved (e.g. Lu et al. 2015). Thus, the tight correlation between the gas metallicity and gas fraction seen in both simulations is likely a result of the subgrid physics that leads to a roughly uniform mixing of metals with the ISM before feedback effects drive gas out from galaxies. The strong (weak) correlation between the gas metallicity and the specific star formation rate

can then be understood as a result of the tight (loose) relation between the cold gas fraction and the specific star formation rate in EAGLE (TNG) discussed above.

3. COMPARISON WITH OBSERVATIONS

3.1. *Observational Sample and Galaxy Properties*

3.1.1. *The xGASS sample*

The GALEX Arecibo SDSS survey (GASS; Catinella et al. 2010) is a targeted HI survey observed with the Arecibo telescope for a sample of galaxies with redshift $0.025 < z < 0.05$ and a flat stellar mass distribution in the range $10^{10} M_{\odot} < M_{*} < 10^{11.5} M_{\odot}$. The GASS sample is randomly selected from a parent sample of 12,000 galaxies located in the overlapping region among SDSS data release 6 (Adelman-McCarthy et al. 2008), GALEX (Martin et al. 2005) Medium Imaging Survey, and the ALFALFA survey footprint. Each galaxy is observed with Arecibo until its HI 21cm emission line is detected or an upper limit of 1.5% of the HI-to-stellar mass ratio (M_{HI}/M_{*}) is reached. The xGASS extends the GASS survey down to a stellar mass lower limit of $10^9 M_{\odot}$, by further observing a sample of galaxies with $10^9 < M_{\text{HI}} < 10^{10.2}$ and $0.01 < z < 0.02$. Here we use the *xGASS representative sample* constructed by Catinella et al. (2018), which includes 1179 galaxies and is representative to the general galaxy population. From this sample, we select central galaxies using the SDSS DR7 group catalog (Yang et al. 2007), and exclude galaxies with $\log \text{sSFR} < -11$ or without gas metallicity measurements (details of $\log \text{sSFR}$ and gas metallicity are described in subsection 3.1.2). The remaining sample contains 278 galaxies with HI detections. We will use this sample for our Random Forest analysis. As shown in the right panel of Figure 1, the xGASS sample has a flat stellar mass distribution and locates in the star-forming sequence with a slope similar to that of the EAGLE sample.

3.1.2. *Galaxy properties*

We consider the following five properties for the random forest analysis of the xGASS sample.

- $\log M_{*}$: logarithm of stellar mass, taken from the NASA-Sloan Atlas ⁴ (NSA; Blanton et al. 2011), estimated by performing a spectral energy distribution (SED) fitting to the SDSS photometry, assuming a Chabrier stellar initial mass function (Chabrier 2003).
- $\log \mu_{*}$: logarithm of stellar surface density, defined as $\log \mu_{*} \equiv \log M_{*}/(2\pi R_{50}^2)$, where R_{50} is the el-

liptical Petrosian half light radius taken from the NSA.

- $u - r$: color index defined by the u band and r band absolute magnitude. The absolute magnitudes are taken from the NSA, measured within an elliptical Petrosian aperture based on GALEX and SDSS images respectively, with Galactic extinction corrected.
- $\log(\text{O}/\text{H}) + 12$: gas phase metallicity, taken from the MPA/JHU SDSS catalog ⁵, derived from SDSS optical spectra using all the most prominent emission lines (Tremonti et al. 2004).
- $\log \sigma_{*}$: logarithm of central stellar velocity dispersion, taken from the MPA/JHU SDSS catalog.

As mentioned above, μ_{*} and $u - r$ are found to be tightly correlated with HI mass fraction in previous studies of HI scaling relations (e.g. Kannappan 2004; Zhang et al. 2009; Li et al. 2022). The other properties, M_{*} , $\log(\text{O}/\text{H}) + 12$ and σ_{*} , are included in order for comparison with the simulations. Due to the lack of measurements, the rest of the properties considered above for the analysis of the simulations are not directly included here. However, some of them are indirectly included through their correlations with the properties selected. These include the sSFR, the stellar metallicity and the black hole mass, which are known to be tightly correlated with $u - r$, $\log(\text{O}/\text{H}) + 12$, and σ_{*} , respectively. This is also the case for $\log V_{\text{max}}$, which is tightly correlated with $\log M_{*}$ according to the well-established stellar-to-halo mass relation of central galaxies in galaxy groups/clusters (Wechsler & Tinker 2018, and references therein). For the black hole accretion rate (\dot{M}_{BH}), it is not immediately clear whether its importance is included indirectly. In order to figure this out, we examined the feature importance of the five properties to \dot{M}_{BH} with the random forest technique. As can be seen from Figure 7, for TNG the surface mass density (μ_{*}) presents the highest importance to \dot{M}_{BH} , while M_{*} , μ_{*} and σ_{*} show similarly high importance in EAGLE. This result implies that, when \dot{M}_{BH} is not included in the random forest analysis, its importance may be inferred from the importance of μ_{*} for TNG and the combination of M_{*} , μ_{*} and σ_{*} for EAGLE. One should keep this result in mind when interpreting the results presented in the following.

3.2. *Feature Importance to the HI Fraction*

⁴ <http://nsatlas.org>

⁵ <https://wwwmpa.mpa-garching.mpg.de>

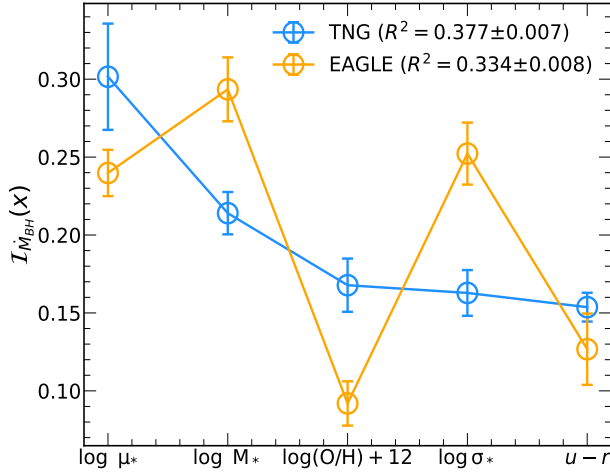


Figure 7. Feature importance with respect to black hole accretion rate in TNG sample.

We perform random forest analyses to determine the importance of the five galaxy properties described above to the HI mass fraction, for both the observational sample xGASS and the EAGLE and TNG simulations. The results are shown in Figure 8. For real galaxies in xGASS, as can be seen, the two most important features are $u - r$ and μ_* . Both M_* and σ_* are ranked quite low, while $\log(\text{O}/\text{H}) + 12$ is in the middle. To make the comparison between simulations and the observation more meaningful, we have trimmed the EAGLE and TNG samples so that they have the same distributions in stellar mass as xGASS. For each simulation we repeat the procedure of sample trimming and the random forest analysis for 40 times. The final importance of each feature and its error are given by the average and the scatter of the 40 subsamples. Furthermore, we have added a “measurement error” to $u - r$, $\log \mu_*$ and $\log(\text{O}/\text{H}) + 12$ in the simulation data, assuming a Gaussian distribution with a full width at half maximum of 0.15, 0.05 and 0.15, respectively. These values are the typical measurement errors in the xGASS sample. We do not attempt to add errors for $\log M_*$ and $\log \sigma_*$ as their importance are too low to affect the result significantly. It should be pointed out, though, that the “errors” added here only represent the lower limits, as real data have more uncertainties (e.g. in the metallicity and in the stellar initial mass function) that are difficult to model reliably. Fortunately, our results remain unchanged even if we completely ignore the errors, suggesting that the results are robust to the uncertainties in the property measurements.

Figure 8 shows that neither of the two simulations can fully reproduce the ranking of feature importance in the xGASS sample. The top-ranked property in both

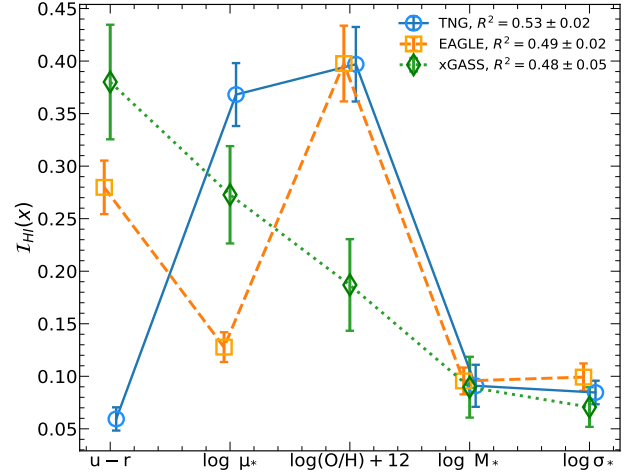


Figure 8. Feature importance of xGASS (green dotted), TNG (blue solid), and EAGLE (orange dashed). For simulation data, the error bar is derived from 40 subsamples that have the same stellar mass distribution as xGASS sample, and the measurement error of $u - r$, $\log \mu_*$, and $\log(\text{O}/\text{H}) + 12$ are considered. A small horizontal shift is added to the lines to avoid overlap.

simulations, $\log(\text{O}/\text{H}) + 12$, is ranked only in the middle in the real sample. TNG is particularly in contrast with the observational data: the top-ranked property $u - r$ in xGASS is now ranked at the bottom. The second-ranked property μ_* in xGASS is now ranked the second in TNG, a result that is largely (if not fully) produced by the importance of black hole accretion rate (\dot{M}_{BH}) found above. Compared to TNG, EAGLE appears to perform better in terms of $u - r$ being ranked second. The low importance of μ_* , M_* and σ_* in EAGLE is consistent with the low importance of \dot{M}_{BH} found above. The gas-phase metallicity remains important (ranks the top) in both simulations, in contrast to the observational data where it ranks the third.

In Figure 9 we show the HI fraction as functions of the five properties in both xGASS (red dots) and the two simulations (black contours). For the simulations we use the full galaxy sample rather than the trimmed subsamples in order for better statistics. We note that the results shown in the figure remain unchanged if any of the subsamples is used instead. Spearman correlation coefficients are indicated in each panel. For xGASS, the HI mass fraction is clearly anti-correlated with $u - r$ and μ_* , with high values of correlation coefficients ($r_s \sim -0.6$). A similar correlation with $u - r$ is seen in EAGLE but not in TNG. The strong correlation with μ_* is seen in TNG but not in EAGLE. The $\log(\text{O}/\text{H}) + 12$ shows the strongest correlation with the HI mass fraction in both simulations. The correlation is weaker in xGASS, particularly towards the low-metallicity end. These results

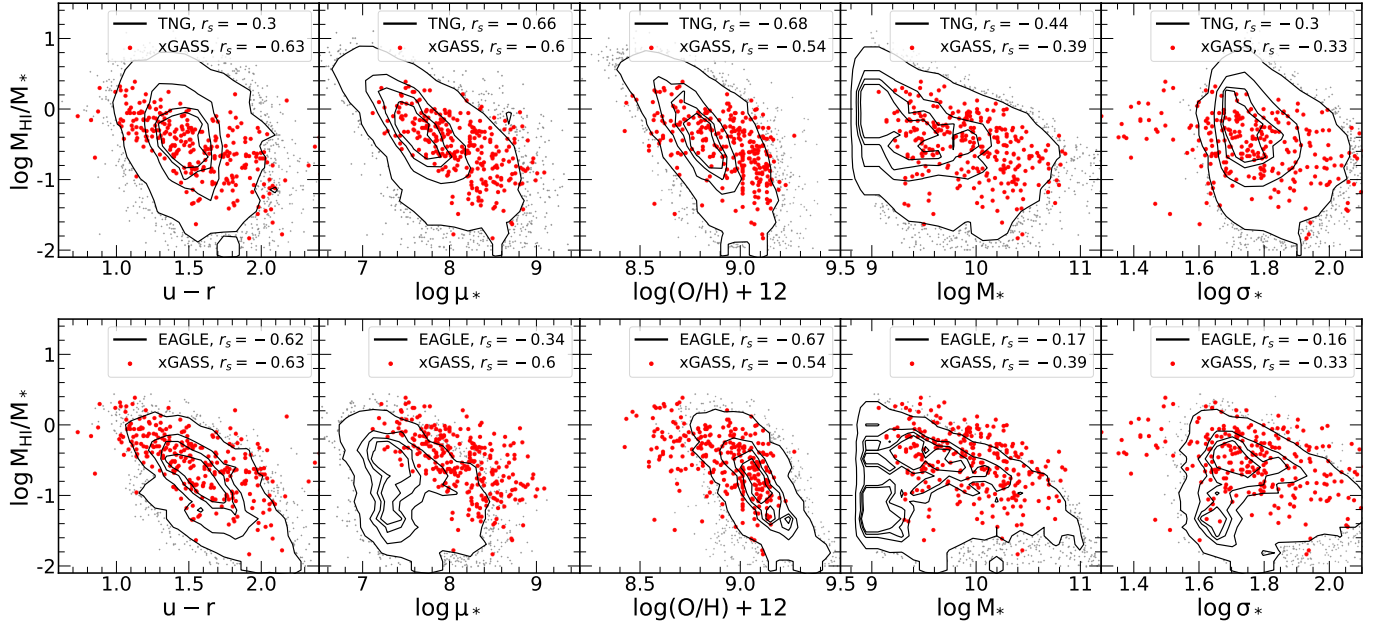


Figure 9. HI fraction as a function of galaxy properties. Contours represent the simulation sample. The red dots represent the xGASS sample. The upper panel shows the TNG sample. The bottom panel shows the EAGLE sample. Spearman correlation coefficient of each sample is shown in the legend.

are well consistent with the rankings of feature importance as shown in the previous figure.

As discussed in [subsection 2.3](#), the different feature importance to the HI fraction as found in the two simulations can be understood in terms of the different feedback processes implemented in the simulations. The fact that the correlation between the HI fraction and the $u-r$ color (a good indicator of the sSFR) predicted by EAGLE is similar to that in xGASS implies that stellar feedback plays a more important role than AGN feedback for the relatively low-mass galaxies studied here. The importance of μ_* in xGASS indicates that feedback processes affecting the cold gas content of a galaxy are correlated with the structure of the galaxy in the central region. As shown earlier, such a correlation is generated in the TNG by the strong dependence of M_{BH} (which determines the strength of AGN feedback) on μ_* . The role of μ_* in EAGLE is much weaker than that in the observation. In principle, more intensive star formation, such as starburst, is expected to be associated with the formation of higher μ_* and with stronger feedback, and so some correlation between the HI mass fraction and μ_* is expected. The discrepancy thus indicates that either EAGLE underestimates such a correlation, or AGN feedback plays a more important role than that assumed in EAGLE, or both. Unfortunately, feedback effects from AGN and starburst are difficult to distinguish by their results for the cold gas content of galaxies. Observational constraints on black hole mass and AGN activities in low-mass galaxies are needed to break the

degeneracy. Finally, the high importance of gas-phase metallicity in both simulations is not seen in xGASS. As discussed above, a tight correlation between the gas-phase metallicity and the gas fraction is expected when metals generated are well mixed with the ISM so that the loss of metal mass in outflows is proportional to that of gas mass. The weaker correlation seen in xGASS thus suggests that the metal and gas in real galaxies are not as tightly coupled as in the simulations.

4. SUMMARY

In this work, we attempt to understand the driving mechanisms for the HI gas content of star-forming central galaxies in the local Universe, by examining two of the current hydrodynamical simulations, IllustrisTNG and EAGLE, as well as the xGASS galaxy sample. Applying the random forest algorithm to a variety of galaxy properties of both simulated and observed galaxies, we obtain the feature importance of the properties to the HI-to-stellar mass ratio (M_{HI}/M_*). In addition, we examine the correlations of M_{HI}/M_* with the galaxy properties, in order to better understand the feature importance, and we compare the results between the two simulations, and between the simulations and the xGASS sample.

Our conclusions are summarized as follows.

- The two simulations behave differently in the random forest analysis. For EAGLE, gas-phase metallicity ($\log(\text{O}/\text{H}) + 12$) and specific star formation

rate (sSFR) are identified as the most important features, and both properties show a tight and negative correlation with the HI mass fraction. For TNG, the two top-ranked properties are black hole accretion rate (\dot{M}_{BH}) and $\log(\text{O}/\text{H}) + 12$, which are also negatively correlated with M_{HI}/M_* . The differences between the two simulations can be understood from the different feedback processes adopted. In EAGLE, the HI content of central galaxies is mainly regulated by stellar feedback, which drives strong gas outflows out to the virial radius of the host halo, thus efficiently suppressing gas inflow and star formation. Consequently, the central supermassive black hole cannot grow efficiently due to the limited gas supply, and AGN feedback is weak and inefficient. In TNG, in contrast, stellar feedback is too weak to efficiently suppress gas inflow, and the black hole is able to grow efficiently and heat the surrounding gas continuously through thermal mode AGN feedback. As a result, in the TNG sample, the regulation of HI content is dominated by the thermal mode AGN feedback.

- Neither simulation can fully reproduce the feature importance of the real galaxies in xGASS, for which the color index of $u - r$ and surface stellar mass density (μ_*) are ranked in the first two places. EAGLE performs better than TNG in the sense that $u - r$ is ranked highly in EAGLE but at the bottom in TNG. This result implies that stellar feedback is likely to play a more dominant role than AGN feedback in driving the HI content of central galaxies at low redshift. Unlike in the simulations, gas-phase metallicity is ranked only mildly for xGASS, suggesting that metals and gas caused by feedback effects in real galaxies is not as tightly coupled as in the simulations.

Our results demonstrate that observations of HI content can provide strong constraints on gas-related sub-grid models in cosmological hydrodynamic simulations, which are able to reproduce both stellar and cold gas content of low-redshift galaxies but using different

recipes. In the next decade spatially resolved HI observations will be available for large samples of galaxies and provide more constraints for the models, thanks to the many new-generation HI surveys (e.g., WALLABY, Koribalski et al. 2020; MIGHTEE-HI, Maddox et al. 2021; LADUMA Blyth et al. 2016).

1 We thank Robert A. Crain for kindly sharing the
 2 HI data of EAGLE. This work is supported by the
 3 National Key R&D Program of China (grant NO.
 4 2022YFA1602902), and the National Natural Science
 5 Foundation of China (grant Nos. 12433003, 11821303,
 6 11973030). This work has made use of the following
 7 software: Numpy (Harris et al. 2020), Scipy (Virtanen
 8 et al. 2020), Scikit-learn (Pedregosa et al. 2011), Mat-
 9 plotlib (Hunter 2007), emcee (Foreman-Mackey et al.
 10 2013), Astropy (Astropy Collaboration et al. 2013, 2018,
 11 2022), and h5py (Collette et al. 2021).

12 Funding for the SDSS and SDSS-II has been pro-
 13 vided by the Alfred P. Sloan Foundation, the Partic-
 14 ipating Institutions, the National Science Foundation,
 15 the U.S. Department of Energy, the National Aeronau-
 16 tics and Space Administration, the Japanese Monbuka-
 17 gakusho, the Max Planck Society, and the Higher Ed-
 18 ucation Funding Council for England. The SDSS Web
 19 Site is <http://www.sdss.org/>.

20 The SDSS is managed by the Astrophysical Research
 21 Consortium for the Participating Institutions. The Par-
 22 ticipating Institutions are the American Museum of Nat-
 23 ural History, Astrophysical Institute Potsdam, Univer-
 24 sity of Basel, University of Cambridge, Case Western
 25 Reserve University, University of Chicago, Drexel Uni-
 26 versity, Fermilab, the Institute for Advanced Study, the
 27 Japan Participation Group, Johns Hopkins University,
 28 the Joint Institute for Nuclear Astrophysics, the Kavli
 29 Institute for Particle Astrophysics and Cosmology, the
 30 Korean Scientist Group, the Chinese Academy of Sci-
 31 ences (LAMOST), Los Alamos National Laboratory, the
 32 Max-Planck-Institute for Astronomy (MPIA), the Max-
 33 Planck-Institute for Astrophysics (MPA), New Mexico
 34 State University, Ohio State University, University of
 35 Pittsburgh, University of Portsmouth, Princeton Uni-
 36 versity, the United States Naval Observatory, and the
 37 University of Washington.

REFERENCES

- Adelman-McCarthy, J. K., Agüeros, M. A., Allam, S. S.,
 et al. 2008, *The Astrophysical Journal Supplement*
 Series, 175, 297, doi: [10.1086/524984](https://doi.org/10.1086/524984)
- Astropy Collaboration, Robitaille, T. P., Tollerud, E. J.,
 et al. 2013, *AAP*, 558, A33,
 doi: [10.1051/0004-6361/201322068](https://doi.org/10.1051/0004-6361/201322068)

- Astropy Collaboration, Price-Whelan, A. M., Sipőcz, B. M., et al. 2018, *AJ*, 156, 123, doi: [10.3847/1538-3881/aabc4f](https://doi.org/10.3847/1538-3881/aabc4f)
- Astropy Collaboration, Price-Whelan, A. M., Lim, P. L., et al. 2022, *ApJ*, 935, 167, doi: [10.3847/1538-4357/ac7c74](https://doi.org/10.3847/1538-4357/ac7c74)
- Ayromlou, M., Nelson, D., & Pillepich, A. 2023, *MNRAS*, 524, 5391, doi: [10.1093/mnras/stad2046](https://doi.org/10.1093/mnras/stad2046)
- Bahé, Y. M., Crain, R. A., Kauffmann, G., et al. 2016, *MNRAS*, 456, 1115, doi: [10.1093/mnras/stv2674](https://doi.org/10.1093/mnras/stv2674)
- Baker, W. M., Maiolino, R., Bluck, A. F. L., et al. 2023, arXiv e-prints, arXiv:2309.00670, doi: [10.48550/arXiv.2309.00670](https://doi.org/10.48550/arXiv.2309.00670)
- Barnes, L. A., & Haehnelt, M. G. 2014, *MNRAS*, 440, 2313, doi: [10.1093/mnras/stu445](https://doi.org/10.1093/mnras/stu445)
- Blanton, M. R., Kazin, E., Muna, D., Weaver, B. A., & Price-Whelan, A. 2011, *AJ*, 142, 31, doi: [10.1088/0004-6256/142/1/31](https://doi.org/10.1088/0004-6256/142/1/31)
- Blitz, L., & Rosolowsky, E. 2006, *ApJ*, 650, 933, doi: [10.1086/505417](https://doi.org/10.1086/505417)
- Bluck, A. F. L., Maiolino, R., Brownson, S., et al. 2022, *A&A*, 659, A160, doi: [10.1051/0004-6361/202142643](https://doi.org/10.1051/0004-6361/202142643)
- Bluck, A. F. L., Piotrowska, J. M., & Maiolino, R. 2023, *ApJ*, 944, 108, doi: [10.3847/1538-4357/acac7c](https://doi.org/10.3847/1538-4357/acac7c)
- Blyth, S., Baker, A. J., Holwerda, B., et al. 2016, in *MeerKAT Science: On the Pathway to the SKA*, 4, doi: [10.22323/1.277.0004](https://doi.org/10.22323/1.277.0004)
- Booth, C. M., & Schaye, J. 2009, *MNRAS*, 398, 53, doi: [10.1111/j.1365-2966.2009.15043.x](https://doi.org/10.1111/j.1365-2966.2009.15043.x)
- Bothwell, M. S., Maiolino, R., Kennicutt, R., et al. 2013, *MNRAS*, 433, 1425, doi: [10.1093/mnras/stt817](https://doi.org/10.1093/mnras/stt817)
- Bower, R. G., Schaye, J., Frenk, C. S., et al. 2017, *MNRAS*, 465, 32, doi: [10.1093/mnras/stw2735](https://doi.org/10.1093/mnras/stw2735)
- Breiman, L. 2001, *Machine Learning*, 45, 5, doi: [10.1023/A:1010933404324](https://doi.org/10.1023/A:1010933404324)
- Calette, A. R., Rodríguez-Puebla, A., Avila-Reese, V., & Lagos, C. d. P. 2021, *MNRAS*, 506, 1507, doi: [10.1093/mnras/stab1788](https://doi.org/10.1093/mnras/stab1788)
- Catinella, B., Schiminovich, D., Kauffmann, G., et al. 2010, *MNRAS*, 403, 683, doi: [10.1111/j.1365-2966.2009.16180.x](https://doi.org/10.1111/j.1365-2966.2009.16180.x)
- Catinella, B., Saintonge, A., Janowiecki, S., et al. 2018, *MNRAS*, 476, 875, doi: [10.1093/mnras/sty089](https://doi.org/10.1093/mnras/sty089)
- Chabrier, G. 2003, *PASP*, 115, 763, doi: [10.1086/376392](https://doi.org/10.1086/376392)
- Chauhan, G., Lagos, C. d. P., Stevens, A. R. H., et al. 2021, *MNRAS*, 506, 4893, doi: [10.1093/mnras/stab1925](https://doi.org/10.1093/mnras/stab1925)
- . 2020, *MNRAS*, 498, 44, doi: [10.1093/mnras/staa2251](https://doi.org/10.1093/mnras/staa2251)
- Collette, A., Kluyver, T., Caswell, T. A., et al. 2021, *h5py/h5py: 3.5.0, 3.5.0*, Zenodo, Zenodo, doi: [10.5281/zenodo.5585380](https://doi.org/10.5281/zenodo.5585380)
- Crain, R. A., Schaye, J., Bower, R. G., et al. 2015, *MNRAS*, 450, 1937, doi: [10.1093/mnras/stv725](https://doi.org/10.1093/mnras/stv725)
- Crain, R. A., Bahé, Y. M., Lagos, C. d. P., et al. 2017, *MNRAS*, 464, 4204, doi: [10.1093/mnras/stw2586](https://doi.org/10.1093/mnras/stw2586)
- Dalla Vecchia, C., & Schaye, J. 2012, *MNRAS*, 426, 140, doi: [10.1111/j.1365-2966.2012.21704.x](https://doi.org/10.1111/j.1365-2966.2012.21704.x)
- Davé, R., Anglés-Alcázar, D., Narayanan, D., et al. 2019, *MNRAS*, 486, 2827, doi: [10.1093/mnras/stz937](https://doi.org/10.1093/mnras/stz937)
- Davé, R., Crain, R. A., Stevens, A. R. H., et al. 2020, *MNRAS*, 497, 146, doi: [10.1093/mnras/staa1894](https://doi.org/10.1093/mnras/staa1894)
- Davies, J. J., Crain, R. A., Oppenheimer, B. D., & Schaye, J. 2020, *MNRAS*, 491, 4462, doi: [10.1093/mnras/stz3201](https://doi.org/10.1093/mnras/stz3201)
- Davis, M., Efstathiou, G., Frenk, C. S., & White, S. D. M. 1985, *ApJ*, 292, 371, doi: [10.1086/163168](https://doi.org/10.1086/163168)
- De Rossi, M. E., Bower, R. G., Font, A. S., Schaye, J., & Theuns, T. 2017, *MNRAS*, 472, 3354, doi: [10.1093/mnras/stx2158](https://doi.org/10.1093/mnras/stx2158)
- Diemer, B., Stevens, A. R. H., Forbes, J. C., et al. 2018, *apjs*, 238, 33, doi: [10.3847/1538-4365/aae387](https://doi.org/10.3847/1538-4365/aae387)
- Diemer, B., Stevens, A. R. H., Lagos, C. d. P., et al. 2019, *MNRAS*, 487, 1529, doi: [10.1093/mnras/stz1323](https://doi.org/10.1093/mnras/stz1323)
- Dubois, Y., Devriendt, J., Slyz, A., & Teyssier, R. 2012, *MNRAS*, 420, 2662, doi: [10.1111/j.1365-2966.2011.20236.x](https://doi.org/10.1111/j.1365-2966.2011.20236.x)
- Ellison, S. L., Patton, D. R., Simard, L., & McConnachie, A. W. 2008, *ApJL*, 672, L107, doi: [10.1086/527296](https://doi.org/10.1086/527296)
- Ellison, S. L., Pan, H.-A., Bluck, A. F. L., et al. 2024, *MNRAS*, 527, 10201, doi: [10.1093/mnras/stad3778](https://doi.org/10.1093/mnras/stad3778)
- Feldmann, R., Quataert, E., Faucher-Giguère, C.-A., et al. 2023, *MNRAS*, 522, 3831, doi: [10.1093/mnras/stad1205](https://doi.org/10.1093/mnras/stad1205)
- Foreman-Mackey, D., Hogg, D. W., Lang, D., & Goodman, J. 2013, *PASP*, 125, 306, doi: [10.1086/670067](https://doi.org/10.1086/670067)
- Genel, S., Vogelsberger, M., Springel, V., et al. 2014, *MNRAS*, 445, 175, doi: [10.1093/mnras/stu1654](https://doi.org/10.1093/mnras/stu1654)
- Gensior, J., Feldmann, R., Reina-Campos, M., et al. 2024, *MNRAS*, 531, 1158, doi: [10.1093/mnras/stae1217](https://doi.org/10.1093/mnras/stae1217)
- Giovanelli, R., Haynes, M. P., Kent, B. R., et al. 2005, *The Astronomical Journal*, 130, 2598, doi: [10.1086/497431](https://doi.org/10.1086/497431)
- Gnedin, N. Y., & Draine, B. T. 2014, *ApJ*, 795, 37, doi: [10.1088/0004-637X/795/1/37](https://doi.org/10.1088/0004-637X/795/1/37)
- Gnedin, N. Y., & Kravtsov, A. V. 2011, *ApJ*, 728, 88, doi: [10.1088/0004-637X/728/2/88](https://doi.org/10.1088/0004-637X/728/2/88)
- Goubert, P. H., Bluck, A. F. L., Piotrowska, J. M., & Maiolino, R. 2024, *MNRAS*, 528, 4891, doi: [10.1093/mnras/stae269](https://doi.org/10.1093/mnras/stae269)
- Grand, R. J. J., van de Voort, F., Zjupa, J., et al. 2019, *MNRAS*, 490, 4786, doi: [10.1093/mnras/stz2928](https://doi.org/10.1093/mnras/stz2928)
- Guo, H., Jones, M. G., Haynes, M. P., & Fu, J. 2020, *ApJ*, 894, 92, doi: [10.3847/1538-4357/ab886f](https://doi.org/10.3847/1538-4357/ab886f)
- Guo, H., Li, C., Zheng, Z., et al. 2017, *ApJ*, 846, 61, doi: [10.3847/1538-4357/aa85e7](https://doi.org/10.3847/1538-4357/aa85e7)

- Harris, C. R., Millman, K. J., van der Walt, S. J., et al. 2020, *Nature*, 585, 357, doi: [10.1038/s41586-020-2649-2](https://doi.org/10.1038/s41586-020-2649-2)
- Hess, K. M., & Wilcots, E. M. 2013, *AJ*, 146, 124, doi: [10.1088/0004-6256/146/5/124](https://doi.org/10.1088/0004-6256/146/5/124)
- Hopkins, P. F. 2015, *MNRAS*, 450, 53, doi: [10.1093/mnras/stv195](https://doi.org/10.1093/mnras/stv195)
- Hopkins, P. F., Kereš, D., Oñorbe, J., et al. 2014, *MNRAS*, 445, 581, doi: [10.1093/mnras/stu1738](https://doi.org/10.1093/mnras/stu1738)
- Huang, S., Haynes, M. P., Giovanelli, R., & Brinchmann, J. 2012, *ApJ*, 756, 113, doi: [10.1088/0004-637X/756/2/113](https://doi.org/10.1088/0004-637X/756/2/113)
- Hughes, T. M., Cortese, L., Boselli, A., Gavazzi, G., & Davies, J. I. 2013, *A&A*, 550, A115, doi: [10.1051/0004-6361/201218822](https://doi.org/10.1051/0004-6361/201218822)
- Hunter, J. D. 2007, *Computing in Science and Engineering*, 9, 90, doi: [10.1109/MCSE.2007.55](https://doi.org/10.1109/MCSE.2007.55)
- Jing, T., & Li, C. 2024, *ApJ*, 975, 17, doi: [10.3847/1538-4357/ad7367](https://doi.org/10.3847/1538-4357/ad7367)
- Jones, M. G., Haynes, M. P., Giovanelli, R., & Moorman, C. 2018, *MNRAS*, 477, 2, doi: [10.1093/mnras/sty521](https://doi.org/10.1093/mnras/sty521)
- Kannappan, S. J. 2004, *ApJL*, 611, L89, doi: [10.1086/423785](https://doi.org/10.1086/423785)
- Koribalski, B. S., Staveley-Smith, L., Westmeier, T., et al. 2020, *APSS*, 365, 118, doi: [10.1007/s10509-020-03831-4](https://doi.org/10.1007/s10509-020-03831-4)
- Krumholz, M. R. 2013, *MNRAS*, 436, 2747, doi: [10.1093/mnras/stt1780](https://doi.org/10.1093/mnras/stt1780)
- Lagos, C. d. P., Theuns, T., Schaye, J., et al. 2016, *MNRAS*, 459, 2632, doi: [10.1093/mnras/stw717](https://doi.org/10.1093/mnras/stw717)
- Leroy, A. K., Walter, F., Brinks, E., et al. 2008, *aj*, 136, 2782, doi: [10.1088/0004-6256/136/6/2782](https://doi.org/10.1088/0004-6256/136/6/2782)
- Li, C., Kauffmann, G., Fu, J., et al. 2012, *MNRAS*, 424, 1471, doi: [10.1111/j.1365-2966.2012.21337.x](https://doi.org/10.1111/j.1365-2966.2012.21337.x)
- Li, N., & Li, C. 2024, *ApJ*, 975, 234, doi: [10.3847/1538-4357/ad7dea](https://doi.org/10.3847/1538-4357/ad7dea)
- Li, X., Li, C., Mo, H. J., Xiao, T., & Wang, J. 2022, *ApJ*, 941, 48, doi: [10.3847/1538-4357/ac9ccb](https://doi.org/10.3847/1538-4357/ac9ccb)
- Lu, Y., Yang, X., Liu, C., et al. 2024, arXiv e-prints, arXiv:2407.18486, doi: [10.48550/arXiv.2407.18486](https://doi.org/10.48550/arXiv.2407.18486)
- Lu, Z., Mo, H. J., & Lu, Y. 2015, *MNRAS*, 450, 606, doi: [10.1093/mnras/stv671](https://doi.org/10.1093/mnras/stv671)
- Ma, W., Liu, K., Guo, H., et al. 2022, *ApJ*, 941, 205, doi: [10.3847/1538-4357/aca326](https://doi.org/10.3847/1538-4357/aca326)
- Maddox, N., Frank, B. S., Ponomareva, A. A., et al. 2021, *AAP*, 646, A35, doi: [10.1051/0004-6361/202039655](https://doi.org/10.1051/0004-6361/202039655)
- Mannucci, F., Cresci, G., Maiolino, R., Marconi, A., & Gnerucci, A. 2010, *MNRAS*, 408, 2115, doi: [10.1111/j.1365-2966.2010.17291.x](https://doi.org/10.1111/j.1365-2966.2010.17291.x)
- Marasco, A., Crain, R. A., Schaye, J., et al. 2016, *MNRAS*, 461, 2630, doi: [10.1093/mnras/stw1498](https://doi.org/10.1093/mnras/stw1498)
- Marinacci, F., Vogelsberger, M., Pakmor, R., et al. 2018, *MNRAS*, 480, 5113, doi: [10.1093/mnras/sty2206](https://doi.org/10.1093/mnras/sty2206)
- Martin, A. M., Giovanelli, R., Haynes, M. P., & Guzzo, L. 2012, *ApJ*, 750, 38, doi: [10.1088/0004-637X/750/1/38](https://doi.org/10.1088/0004-637X/750/1/38)
- Martin, A. M., Papastergis, E., Giovanelli, R., et al. 2010, *ApJ*, 723, 1359, doi: [10.1088/0004-637X/723/2/1359](https://doi.org/10.1088/0004-637X/723/2/1359)
- Martin, D. C., Fanson, J., Schiminovich, D., et al. 2005, *The Astrophysical Journal*, 619, L1, doi: [10.1086/426387](https://doi.org/10.1086/426387)
- Meyer, M. J., Zwaan, M. A., Webster, R. L., Brown, M. J. I., & Staveley-Smith, L. 2007, *ApJ*, 654, 702, doi: [10.1086/508799](https://doi.org/10.1086/508799)
- Meyer, M. J., Zwaan, M. A., Webster, R. L., et al. 2004, *MNRAS*, 350, 1195, doi: [10.1111/j.1365-2966.2004.07710.x](https://doi.org/10.1111/j.1365-2966.2004.07710.x)
- Mitchell, P. D., Schaye, J., Bower, R. G., & Crain, R. A. 2020, *MNRAS*, 494, 3971, doi: [10.1093/mnras/staa938](https://doi.org/10.1093/mnras/staa938)
- Mo, H., van den Bosch, F. C., & White, S. 2010, *Galaxy Formation and Evolution*
- Naiman, J. P., Pillepich, A., Springel, V., et al. 2018, *MNRAS*, 477, 1206, doi: [10.1093/mnras/sty618](https://doi.org/10.1093/mnras/sty618)
- Nelson, D., Pillepich, A., Springel, V., et al. 2018, *MNRAS*, 475, 624, doi: [10.1093/mnras/stx3040](https://doi.org/10.1093/mnras/stx3040)
- Obreschkow, D., Glazebrook, K., Kilborn, V., & Lutz, K. 2016, *ApJL*, 824, L26, doi: [10.3847/2041-8205/824/2/L26](https://doi.org/10.3847/2041-8205/824/2/L26)
- Obuljen, A., Alonso, D., Villaescusa-Navarro, F., Yoon, I., & Jones, M. 2019, *MNRAS*, 486, 5124, doi: [10.1093/mnras/stz1118](https://doi.org/10.1093/mnras/stz1118)
- Papastergis, E., Giovanelli, R., Haynes, M. P., Rodríguez-Puebla, A., & Jones, M. G. 2013, *ApJ*, 776, 43, doi: [10.1088/0004-637X/776/1/43](https://doi.org/10.1088/0004-637X/776/1/43)
- Paul, N., Choudhury, T. R., & Paranjape, A. 2018, *MNRAS*, 479, 1627, doi: [10.1093/mnras/sty1539](https://doi.org/10.1093/mnras/sty1539)
- Pedregosa, F., Varoquaux, G., Gramfort, A., et al. 2011, *Journal of Machine Learning Research*, 12, 2825
- Pillepich, A., Nelson, D., Hernquist, L., et al. 2018, *MNRAS*, 475, 648, doi: [10.1093/mnras/stx3112](https://doi.org/10.1093/mnras/stx3112)
- Piotrowska, J. M., Bluck, A. F. L., Maiolino, R., & Peng, Y. 2022, *MNRAS*, 512, 1052, doi: [10.1093/mnras/stab3673](https://doi.org/10.1093/mnras/stab3673)
- Planck Collaboration, Ade, P. A. R., Aghanim, N., et al. 2014, *AAP*, 571, A1, doi: [10.1051/0004-6361/201321529](https://doi.org/10.1051/0004-6361/201321529)
- . 2016, *AAP*, 594, A13, doi: [10.1051/0004-6361/201525830](https://doi.org/10.1051/0004-6361/201525830)
- Reina-Campos, M., Keller, B. W., Kruijssen, J. M. D., et al. 2022, *MNRAS*, 517, 3144, doi: [10.1093/mnras/stac1934](https://doi.org/10.1093/mnras/stac1934)
- Rhee, J., Meyer, M., Popping, A., et al. 2023, *MNRAS*, 518, 4646, doi: [10.1093/mnras/stac3065](https://doi.org/10.1093/mnras/stac3065)
- Saraf, M., Cortese, L., Wong, O. I., et al. 2024, *MNRAS*, 530, 2420, doi: [10.1093/mnras/stae942](https://doi.org/10.1093/mnras/stae942)
- Schaye, J., & Dalla Vecchia, C. 2008, *MNRAS*, 383, 1210, doi: [10.1111/j.1365-2966.2007.12639.x](https://doi.org/10.1111/j.1365-2966.2007.12639.x)
- Schaye, J., Crain, R. A., Bower, R. G., et al. 2015, *MNRAS*, 446, 521, doi: [10.1093/mnras/stu2058](https://doi.org/10.1093/mnras/stu2058)

- Sijacki, D., Vogelsberger, M., Genel, S., et al. 2015, MNRAS, 452, 575, doi: [10.1093/mnras/stv1340](https://doi.org/10.1093/mnras/stv1340)
- Springel, V. 2005, MNRAS, 364, 1105, doi: [10.1111/j.1365-2966.2005.09655.x](https://doi.org/10.1111/j.1365-2966.2005.09655.x)
- . 2010, MNRAS, 401, 791, doi: [10.1111/j.1365-2966.2009.15715.x](https://doi.org/10.1111/j.1365-2966.2009.15715.x)
- Springel, V., & Hernquist, L. 2003, MNRAS, 339, 289, doi: [10.1046/j.1365-8711.2003.06206.x](https://doi.org/10.1046/j.1365-8711.2003.06206.x)
- Springel, V., White, S. D. M., Tormen, G., & Kauffmann, G. 2001, MNRAS, 328, 726, doi: [10.1046/j.1365-8711.2001.04912.x](https://doi.org/10.1046/j.1365-8711.2001.04912.x)
- Springel, V., Pakmor, R., Pillepich, A., et al. 2018, MNRAS, 475, 676, doi: [10.1093/mnras/stx3304](https://doi.org/10.1093/mnras/stx3304)
- Sternberg, A., Le Petit, F., Roueff, E., & Le Bourlot, J. 2014, ApJ, 790, 10, doi: [10.1088/0004-637X/790/1/10](https://doi.org/10.1088/0004-637X/790/1/10)
- Stevens, A. R. H., Diemer, B., Lagos, C. d. P., et al. 2019, MNRAS, 483, 5334, doi: [10.1093/mnras/sty3451](https://doi.org/10.1093/mnras/sty3451)
- Trayford, J. W., Theuns, T., Bower, R. G., et al. 2015, MNRAS, 452, 2879, doi: [10.1093/mnras/stv1461](https://doi.org/10.1093/mnras/stv1461)
- Tremonti, C. A., Heckman, T. M., Kauffmann, G., et al. 2004, ApJ, 613, 898, doi: [10.1086/423264](https://doi.org/10.1086/423264)
- Villaescusa-Navarro, F., Genel, S., Castorina, E., et al. 2018, ApJ, 866, 135, doi: [10.3847/1538-4357/aadba0](https://doi.org/10.3847/1538-4357/aadba0)
- Virtanen, P., Gommers, R., Oliphant, T. E., et al. 2020, Nature Methods, 17, 261, doi: [10.1038/s41592-019-0686-2](https://doi.org/10.1038/s41592-019-0686-2)
- Vogelsberger, M., Genel, S., Springel, V., et al. 2014a, Nature, 509, 177, doi: [10.1038/nature13316](https://doi.org/10.1038/nature13316)
- . 2014b, MNRAS, 444, 1518, doi: [10.1093/mnras/stu1536](https://doi.org/10.1093/mnras/stu1536)
- Ward, S. R., Harrison, C. M., Costa, T., & Mainieri, V. 2022, MNRAS, 514, 2936, doi: [10.1093/mnras/stac1219](https://doi.org/10.1093/mnras/stac1219)
- Watts, A. B., Power, C., Catinella, B., Cortese, L., & Stevens, A. R. H. 2020, MNRAS, 499, 5205, doi: [10.1093/mnras/staa3200](https://doi.org/10.1093/mnras/staa3200)
- Wechsler, R. H., & Tinker, J. L. 2018, ARA&A, 56, 435, doi: [10.1146/annurev-astro-081817-051756](https://doi.org/10.1146/annurev-astro-081817-051756)
- Weinberger, R., Springel, V., Hernquist, L., et al. 2017, MNRAS, 465, 3291, doi: [10.1093/mnras/stw2944](https://doi.org/10.1093/mnras/stw2944)
- White, S. D. M., & Rees, M. J. 1978, MNRAS, 183, 341, doi: [10.1093/mnras/183.3.341](https://doi.org/10.1093/mnras/183.3.341)
- Wright, R. J., Somerville, R. S., Lagos, C. d. P., et al. 2024, MNRAS, 532, 3417, doi: [10.1093/mnras/stae1688](https://doi.org/10.1093/mnras/stae1688)
- Yang, H., Liao, S., Fattahi, A., et al. 2024, arXiv e-prints, arXiv:2408.09784, doi: [10.48550/arXiv.2408.09784](https://doi.org/10.48550/arXiv.2408.09784)
- Yang, X., Mo, H. J., van den Bosch, F. C., et al. 2007, ApJ, 671, 153, doi: [10.1086/522027](https://doi.org/10.1086/522027)
- York, D. G., Adelman, J., Anderson, John E., J., et al. 2000, AJ, 120, 1579, doi: [10.1086/301513](https://doi.org/10.1086/301513)
- Zahid, H. J., Dima, G. I., Kudritzki, R.-P., et al. 2014, ApJ, 791, 130, doi: [10.1088/0004-637X/791/2/130](https://doi.org/10.1088/0004-637X/791/2/130)
- Zerbo, M. C., De Rossi, M. E., Lara-López, M. A., Cora, S. A., & Zenocрати, L. J. 2024, MNRAS, 528, 7509, doi: [10.1093/mnras/stae490](https://doi.org/10.1093/mnras/stae490)
- Zhang, W., Li, C., Kauffmann, G., et al. 2009, MNRAS, 397, 1243, doi: [10.1111/j.1365-2966.2009.15050.x](https://doi.org/10.1111/j.1365-2966.2009.15050.x)
- Zinger, E., Pillepich, A., Nelson, D., et al. 2020, MNRAS, 499, 768, doi: [10.1093/mnras/staa2607](https://doi.org/10.1093/mnras/staa2607)
- Zu, Y. 2020, MNRAS, 496, 111, doi: [10.1093/mnras/staa1457](https://doi.org/10.1093/mnras/staa1457)
- Zwaan, M. A., Meyer, M. J., Staveley-Smith, L., & Webster, R. L. 2005, MNRAS, 359, L30, doi: [10.1111/j.1745-3933.2005.00029.x](https://doi.org/10.1111/j.1745-3933.2005.00029.x)